Supporting Material

The electrostatics of deformable lipid membranes

Igor Vorobyov, Borislava Bekker and Toby W. Allen

<div style="text-align:center">

Supporting Material for
"The electrostatics of deformable lipid membranes"

Igor Vorobyov, Borislava Bekker and Toby W. Allen.
Department of Chemistry, University of California, Davis. U.S.A.

</div>

Supporting Material Text

<u>Additional simulation methods</u>

The CHARMM program (1) was used for all molecular dynamics (MD) simulations with the CHARMM27 (C27) force field for lipids (2), proteins (3), TIP3P water (4) and ions (5). All non-polarizable simulations employed a 2 fs time step, whereas a 1 fs time step was used for polarizable models. Coordinates were saved every 100 time steps for analysis. Bonds to H atoms were constrained using SHAKE (6). Non-polarizable MD simulations used the leapfrog integrator (7), with Nose-Hoover thermostat (8) and Langevin piston method for pressure coupling (9). A classical Drude oscillator model (10, 11) was used in which Drude positions were adjusted self-consistently in the electric field of other atoms or propagated in MD simulations via an extended Lagrangian formalism through the assignment of a small mass (0.4 amu) at low temperature (1 K) using a separate thermostat. (11) The new velocity Verlet integrator (11), Nose-Hoover thermostat (8) and modified Hoover-Anderson barostat (11, 12) were employed for polarizable simulations. Lipid bilayer systems were simulated at 330 K in the NP_nAT ensemble using a constant pressure of 1 atm, parallel to the bilayer normal. The lateral box dimensions were based on the experimental area per lipid of ~64 $Å^2$ for DPPC (13) and ~60 $Å^2$ for DMPC(14), accounting for solute or peptide volume.

In all MD simulations, periodic boundary conditions (PBC) were imposed. Electrostatic interactions were calculated using particle-mesh Ewald (PME) summation (15), with a coupling parameter 0.34 and 6-th order spline for mesh interpolation. For systems carrying a net charge, corresponding energy and pressure corrections were applied (16). Non-bond pair lists were maintained out to 16 Å, and a real space cutoff of 10 Å was used via an atom-based energy shift algorithm (17). The effect of cutoff scheme has no substantial differences in bilayer properties (18).

Continuum electrostatics calculations were performed using the PBEQ module of CHARMM. These calculations were performed for methyl-guanidinium ($MGuanH^+$), valinomycin (VM) and gramicidin A (gA) models. In continuum membrane calculations the $MGuanH^+$ was placed at various positions, with the center of mass spanning the membrane, and Poisson's equation was solved. The membrane was assigned a 25 Å-thick core of dielectric constant 2 (as it would be with the polarizable MD force field) or 1 (non-polarizable case), while interfacial regions were assigned an aqueous dielectric constant of 80. The system was placed in a large box of dimensions 50x50x100 Å. The grid size 0.5 Å was used, with results found to be invariant to 0.10 Å changes. Dielectric constants were assigned with a water-sized reentrant probe after assigning Born radii (19, 20). For $MGuanH^+$ atoms completely inside the membrane core (with |z|≤10 Å), a methylene-sized probe and scaled Lennard-Jones radii were used. In the absence of the contribution from a peptide's charge distribution, the dielectric response of the protein can be approximated by an implicit dielectric constant, ε_p. The choice of ε_p depends on the specific protein environment as well as model parameters, making it a fairly ambiguous parameter. A range of ε_p from 1 to 5 was explored for $MGuanH^+$, as in the previous work (21). For VM and gA models, the approximate value of ε_p was determined from MD simulations using either induced polarization or peptide dipole fluctuations for a spherical or ellipsoidal geometry, as detailed below.

For VM and gA continuum electrostatics calculations with Poisson-Boltzmann solver in PBEQ module of CHARMM were used to calculate the effect of the peptide dielectric constant ε_p on the electrostatic potential across the membrane with peptide charges turned off. A reduced set of MD trajectory frames has been used (1500 for VM and 100 for gA). Periodic boundary conditions were used for VM calculations (with those in *xy* plane suppressed) whereas explicit first-shell image atoms in all directions were used for gA system (resulting in a system of 129,900 atoms for C27 and 140,070 atoms from Drude polarizable gA simulations). A grid size of 0.5 Å in all directions and bilinear interpolation for boundary potentials were used. All charges on VM or gA and channel water were set to 0 and a dielectric constant ε_p from 1 to 5 for VM or gA has been assigned to that region. Values of ε_p were mapped out with a water-sized reentrant probe after assigning Born radii (19, 20). For peptide atoms completely inside the membrane core (with $|z| \leq 10$ Å), a methylene-sized probe was used. The channel water for gA calculations was defined to be all water molecules with their oxygen atoms inside a cylinder of height 25 Å and radius 3 Å oriented on the channel axis. The channel axis was aligned with z axis and was defined as a vector connecting centers of mass of backbone non-hydrogen atoms for two gA subunits. The center of mass of gA backbone non-H atoms was set at the origin. For VM, the system was oriented (without rotation) with origin at the center of the 6 ester carbonyl oxygen atoms (the putative K^+ binding site).

Estimation of valinomycin and gramicidin A dielectric constants

The dielectric constants of VM and gA were estimated by two different methods using vacuum or existing membrane simulations. In both methods VM was assumed to have a spherical geometry, while gA an ellipsoidal one (acknowledging these are just rough estimates for the purposes of qualitative or semi-quantitative discussions in the main text). Additionally, in the case of gA, seven water molecules were maintained inside the protein pore for the duration of the simulations. The first method was based on the dipole fluctuations, which were obtained from 100 ns simulation of each peptide in vacuum. The dielectric constant was calculated using (22):

$$\frac{\langle\mu^2\rangle - \langle\mu\rangle^2}{3\varepsilon_0 VkT} = \frac{\varepsilon - 1}{1 + (\varepsilon - 1)A},$$

where μ is the total dipole moment, V is the estimated volume of the molecule, k is Boltzmann constant and T is temperature. For a general case, the constant A, which depends on the boundary conditions is defined as (23)

$$\frac{abc}{2} \int_0^\infty \frac{ds}{(s+a^2)^{3/2}(s+b^2)^{1/2}(s+c^2)^{1/2}},$$

where a, b and c are the principal axes. When $a=b=c$, A becomes 1/3 and the expression for spherical geometry is obtained. A was estimated to be 0.124 in the case of gA with $a/b=2.4$ and b and c equal. In the second method a separate 100 ns simulation was carried out with an applied electric field of 0.02 V/Å in the z-direction and the expression used to evaluate ε was (22)

$$\frac{\langle P_z\rangle}{\mathbf{E}_0\varepsilon_0} = \frac{\varepsilon - 1}{1 + (\varepsilon - 1)A},$$

where P_z is the polarization (i.e. the dipole moment z component, μ_z, per unit volume) in the z direction, $\mathbf{E}_0$ is the applied electric field and A is defined as above (23). The results of these calculations along with corresponding standard errors of the mean from block averaging are summarized in Table below. The time series of ε, dipole fluctuations ($\langle\mu^2\rangle - \langle\mu\rangle^2$), and $\langle\mu_z\rangle$ are shown in Figure S14 demonstrating convergence,

Protein	Fluctuating Dipole	Applied Field
VM	1.83±0.17	1.94±0.35
gA	4.00±0.48	4.72±1.19

The estimated dielectric constant for gA obtained using fluctuating dipole method is consistent with previous experimental estimate of the dielectric constant of 4 for this peptide (24). For VM the fluctuating dipole estimate from simulations in vacuum is very similar to that obtained from MD simulations of VM constrained at the bilayer center using fully atomistic C27 simulations (described in the main text) and the same methodology to estimate ε. Therefore peptide dielectric constants of 2 and 4 were used as the best estimates for C27 gA and VM models noting, however, some ambiguities in the definition of protein dielectric constant (25). Note also that these values are likely to be different (higher) when using polarizable models for these peptides.

Size correction for gA channel PMF calculation with polarizable membrane

A free energy cycle (Scheme S1), similar to that used in ref. (26) but for a polarizable membrane, was created in order to estimate a size correction for the MD simulation of gA using C27+pol2 model. The corrected PMF for ion permeation through gA was used in calculations of channel flux and equilibrium dissociation constant, K_D, using the same methods as in (26). The calculated value of K_D is 0.077 M, which is in excellent agreement with the experimental result of 0.07 M (26). The maximum conductance of gA, which is governed by corrected PMF, was evaluated using a 1D single-ion Nernst Planck theory of Levitt ((26) and references therein) and the value was found to be 1.9 pS, slightly lower than the experimental value of 21 pS (27).
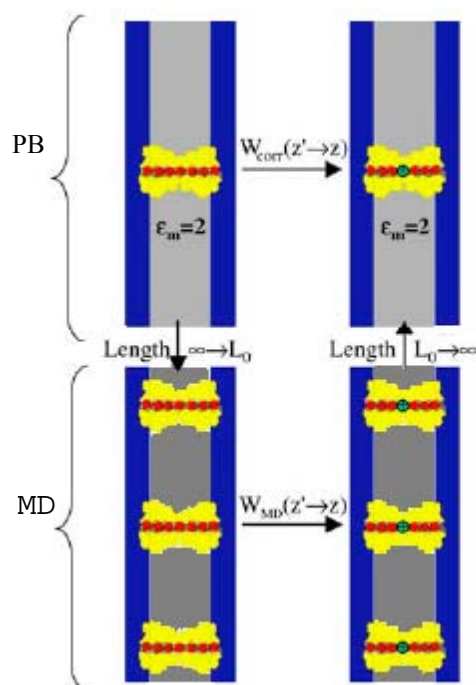
Scheme S1. Free energy cycle illustrating the size correction calculation when the PMF was obtained using finite system size. The gA channel is shown in yellow, high dielectric (ε=80) bulk water in blue and hydrocarbon in grey.

Supporting Material References

1. Brooks, B. R., R. E. Bruccoleri, B. D. Olafson, D. J. States, S. Swaminathan *et al.* 1983. CHARMM - a Program for Macromolecular Energy, Minimization, and Dynamics Calculations. *J.Comput. Chem.* 4:187-217.
2. Feller, S. E., and A. D. MacKerell. 2000. An improved empirical potential energy function for molecular simulations of phospholipids. *J. Phys. Chem. B* 104:7510-7515.
3. MacKerell, A. D., D. Bashford, M. Bellott, R. L. Dunbrack, J. D. Evanseck *et al.* 1998. All-atom empirical potential for molecular modeling and dynamics studies of proteins. *J. Phys. Chem. B* 102:3586-3616.
4. Jorgensen, W. L., J. Chandrasekhar, J. D. Madura, R. W. Impey, and M. L. Klein. 1983. Comparison of Simple Potential Functions for Simulating Liquid Water. *J. Chem. Phys.* 79:926-935.
5. Beglov, D., and B. Roux. 1994. Finite Representation of an Infinite Bulk System - Solvent Boundary Potential for Computer-Simulations. *J. Chem. Phys.* 100:9050-9063.
6. Ryckaert, J. P., G. Ciccotti, and H. J. C. Berendsen. 1977. Numerical Integration of Cartesian Equations of Motion of a System with Constraints: Molecular Dynamics of N-Alkanes. *J. Comput. Phys.* 23:327-341.
7. Allen, M. P., and D. J. Tildesley. 1987. Computer Simulation of Liquids. Clarendon Press, Oxford.
8. Hoover, W. G. 1985. Canonical Dynamics - Equilibrium Phase-Space Distributions. *Phys. Rev. A* 31:1695-1697.
9. Feller, S. E., Y. H. Zhang, R. W. Pastor, and B. R. Brooks. 1995. Constant-Pressure MolecularDynamics Simulation - the Langevin Piston Method. *J. Chem. Phys.* 103:4613-4621.
10. Anisimov, V. M., G. Lamoureux, I. V. Vorobyov, N. Huang, B. Roux *et al.* 2005. Determination of electrostatic parameters for a polarizable force field based on the classical Drude oscillator. *J. Chem. Theory Comput.* 1:153-168.
11. Lamoureux, G., and B. Roux. 2003. Modeling induced polarization with classical Drude oscillators: Theory and molecular dynamics simulation algorithm. *J. Chem. Phys.* 119:3025-3039.
12. Martyna, G. J., M. E. Tuckerman, D. J. Tobias, and M. L. Klein. 1996. Explicit reversible integrators for extended systems dynamics. *Molecular Physics* 87:1117-1157.
13. Kucerka, N., S. Tristram-Nagle, and J. F. Nagle. 2006. Closer look at structure of fully hydrated fluid phase DPPC bilayers. *Biophys. J.* 90:L83-L85.
14. Kucerka, N., Y. F. Liu, N. J. Chu, H. I. Petrache, S. T. Tristram-Nagle *et al.* 2005. Structure of fully hydrated fluid phase DMPC and DLPC lipid bilayers using X-ray scattering from oriented multilamellar arrays and from unilamellar vesicles. *Biophys. J.* 88:2626-2637.
15. Darden, T., D. York, and L. Pedersen. 1993. Particle Mesh Ewald - an N.Log(N) Method for Ewald Sums in Large Systems. *J. Chem. Phys.* 98:10089-10092.
16. Bogusz, S., T. E. Cheatham, and B. R. Brooks. 1998. Removal of pressure and free energy artifacts in charged periodic systems via net charge corrections to the Ewald potential. *J. Chem. Phys.* 108:7070-7084.
17. Steinbach, P. J., and B. R. Brooks. 1994. New Spherical-Cutoff Methods for Long-Range Forces in Macromolecular Simulation. *J. Comput. Chem.* 15:667-683.
18. Vorobyov, I., and T. W. Allen. 2010. The electrostatics of solvent and membrane interfaces and the role of electronic polarizability. *J. Chem. Phys.* 132:185101.
19. Nina, M., W. Im, and B. Roux. 1999. Optimized atomic radii for protein continuum electrostatics solvation forces. *Biophys. Chem.* 78:89-96.
20. Allen, T. W., O. S. Andersen, and B. Roux. 2004. On the importance of atomic fluctuations, protein flexibility, and solvent in ion permeation. *J. Gen. Physiol.* 124:679-690.

21. Vorobyov, I., L. B. Li, and T. W. Allen. 2008. Assessing atomistic and coarse-grained force fields for protein-lipid interactions: The formidable challenge of an ionizable side chain in a membrane. *J. Phys. Chem. B* 112:9588-9602.

22. Neumann, M. 1983. Dipole moment fluctuation formulas in computer simulations of polar systems. *Mol. Phys.* 50:841-858.

23. Böttcher, C. J. F., ,O. C. van Belle, P. Bordewijk, and A. Rip. 1973. Theory of electric polarization. Elsevier Scientific Pub. Co., Amsterdam, New York.

24. Jordan, P. C. 1984. The Total Electrostatic Potential in a Gramicidin Channel. *J. Membrane Biol.* 78:91-102.

25. Warshel, A., P. K. Sharma, M. Kato, and W. W. Parson. 2006. Modeling electrostatic effects in proteins. *Biochim. Biophys. Acta-Proteins Proteomics* 1764:1647-1676.

26. Allen, T. W., O. S. Andersen, and B. Roux. 2006. Ion permeation through a narrow channel: Using gramicidin to ascertain all-atom molecular dynamics potential of mean force methodology and biomolecular force fields. *Biophys. J.* 90:3447-3468.

27. Busath, D. D., C. D. Thulin, R. W. Hendershot, L. R. Phillips, P. Maughan *et al.* 1998. Noncontact dipole effects on channel permeation. I. Experiments with (5F-indole)Trp13 gramicidin A channels. *Biophys J.* 75:2830-2844.

28. Aksimentiev, A., and K. Schulten. 2005. Imaging alpha-hemolysin with molecular dynamics: Ionic conductance, osmotic permeability, and the electrostatic potential map. *Biophys. J.* 88:3745-3761.

29. Humphrey, W., A. Dalke, and K. Schulten. 1996. VMD: Visual molecular dynamics. *J. Mol. Graph.* 14:33-38.

30. Wilson, M. A., A. Pohorille, and L. R. Pratt. 1988. Surface Potential of the Water Liquid-Vapor Interface. *J. Chem. Phys.* 88:3281-3285.

31. Macias, A. T., and A. D. MacKerell. 2005. CH/pi interactions involving aromatic amino acids: Refinement of the CHARMM tryptophan force field. *J. Comput. Chem.* 26:1452-1463.

Table S1. Electrostatic parameters of lipid models

Lipid tail parameters	C27	Drude	
		C27+pol1	C27+pol2
q(C) in CH_3	-0.270	-0.177	-0.270
q(C) in CH_2	-0.180	-0.156	-0.180
q(H) in CH_3	0.090	0.059	0.090
q(H) in CH_2	0.090	0.078	0.090
α(C) in CH_3		2.051	2.051
α(C) in CH_2		1.660	1.660
q(C22,C32)	-0.080	-0.056	-0.080
lipid polarizable atoms	none	C22-C216 C32-C316	C23-C216 C33-C316

q are partial atomic charges in units of e; α are atomic polarizabilities in Å^3. Standard C27 parameters were used for other lipid atoms in all models. Atoms C22 and C32 are the first carbon atoms of lipid tails (ones adjacent to carbonyl C) for sn-2 and sn-1 chains, respectively (while C216 and C316 are the last C atoms).

Table S2. Properties of the perturbed lipid bilayer with water defects at the center.

R_{sph}	$<\sigma>$		$<z>$		$<d_{PP}>$		$<d_{CC}>$		$<U_{cons}>$	
0	11.63 ±	1.49	83.57 ±	0.02	39.12 ±	0.08	29.75 ±	0.06	0.01 ±	0.00
2	14.11 ±	1.48	83.55 ±	0.02	39.16 ±	0.07	29.81 ±	0.05	0.15 ±	0.00
3	14.67 ±	0.65	83.59 ±	0.02	39.29 ±	0.06	29.91 ±	0.04	0.28 ±	0.02
4	12.89 ±	1.10	83.47 ±	0.02	39.46 ±	0.03	29.98 ±	0.03	0.48 ±	0.03
5	13.59 ±	0.71	83.27 ±	0.04	39.61 ±	0.07	30.26 ±	0.07	1.29 ±	0.11
6	11.39 ±	1.04	82.89 ±	0.01	39.50 ±	0.16	30.54 ±	0.10	2.07 ±	0.07
7	1.78 ±	2.29	82.47 ±	0.08	39.59 ±	0.10	30.78 ±	0.08	2.83 ±	0.13
8	2.48 ±	1.20	81.88 ±	0.01	39.77 ±	0.11	31.41 ±	0.05	3.78 ±	0.02
9	-3.79 ±	1.28	81.33 ±	0.02	39.68 ±	0.32	31.51 ±	0.23	4.81 ±	0.12
10	-4.96 ±	1.30	80.56 ±	0.04	40.21 ±	0.10	31.98 ±	0.10	6.17 ±	0.07

R_{sph} – radius of the water sphere in Å; $<\sigma>$ - average surface tension in dyn/cm; $<z>$ - average height of simulation box in Å; $<d_{PP}>$ - average bilayer thickness in Å measured as average distance between P atom vertical positions in 2 leaflets; $<d_{CC}>$ - average bilayer thickness in Å, measured as average distance between carbonyl C atom vertical positions in 2 leaflets; $<U_{cons}>$ - average energy of constraint (in kcal/mol) holding a water sphere at the bilayer center. Uncertainties were determined as standard errors of the mean from block averaging.

Table S3. Average number of polar species inside the hydrophobic membrane core from the perturbed lipid bilayer simulations with water defects at the center.

R_{sph}	water O				K^+			Cl^-			lipid P			lipid N		
	constr	aver	min	max	aver	min	max	aver	min	max	aver	min	max	aver	min	max
0	0	7.5	0	28	0.00	0	0	0.00	0	0	0.01	0	2	0.04	0	2
2	1	9.5	1	31	0.00	0	1	0.00	0	0	0.04	0	2	0.03	0	2
3	4	11.7	4	32	0.00	0	1	0.00	0	1	0.01	0	2	0.00	0	2
4	9	17.9	9	40	0.00	0	1	0.00	0	0	0.01	0	1	0.00	0	2
5	18	41.2	23	78	0.00	0	1	0.00	0	0	0.50	0	4	0.31	0	3
6	30	72.4	49	104	0.00	0	1	0.03	0	1	1.65	0	6	1.19	0	4
7	48	108.5	72	152	0.17	0	2	0.11	0	2	2.22	0	7	1.56	0	5
8	72	152.7	115	197	0.04	0	2	0.04	0	1	2.69	0	7	2.16	0	6
9	102	193.4	158	242	0.74	0	3	0.14	0	1	4.17	0	9	3.05	0	8
10	140	244.7	210	286	0.81	0	3	0.15	0	2	3.49	0	8	2.33	0	6

R_{sph} – radius of the water sphere in Å. The hydrophobic membrane core was defined as $|z| \leq 13$ Å with respect to the bilayer center of mass. Maximum (max), minimum (min) and average (aver) numbers of the corresponding species refer to those from all analyzed data

Table S4. Maximum extent of penetration of some polar species to the hydrophobic membrane core from perturbed lipid bilayer simulations with water defect at the center.

R_{sph}	lipid P			K^+			Cl^-		
	aver	min	max	aver	min	max	aver	min	max
0									
2	15.1	9.4	17.8	20.1	12.6	28.1	22.9	14.8	29.6
3	15.2	11.5	17.7	19.3	12.3	28.0	23.1	12.0	29.7
4	15.4	10.6	17.8	19.8	12.0	27.5	23.2	13.6	29.5
5	12.6	4.1	17.9	20.3	12.7	27.9	23.1	15.0	29.7
6	9.5	3.1	15.9	20.1	11.2	29.5	22.8	3.8	29.7
7	9.3	4.0	17.4	17.8	0.0	28.3	20.5	0.0	29.0
8	9.3	3.2	15.3	19.7	0.0	27.3	22.0	0.0	30.4
9	8.9	3.3	14.4	11.3	0.0	27.2	19.2	0.0	29.5
10	9.7	4.2	13.8	9.2	0.0	25.3	19.4	0.0	30.1

R_{sph} – radius of the water sphere in Å. All positions are in Å relative the bilayer center of mass and were determined for each analyzed frame of the simulation. Maximum (max), minimum (min) and average (aver) positions of the corresponding atoms refer to those from all analyzed data.
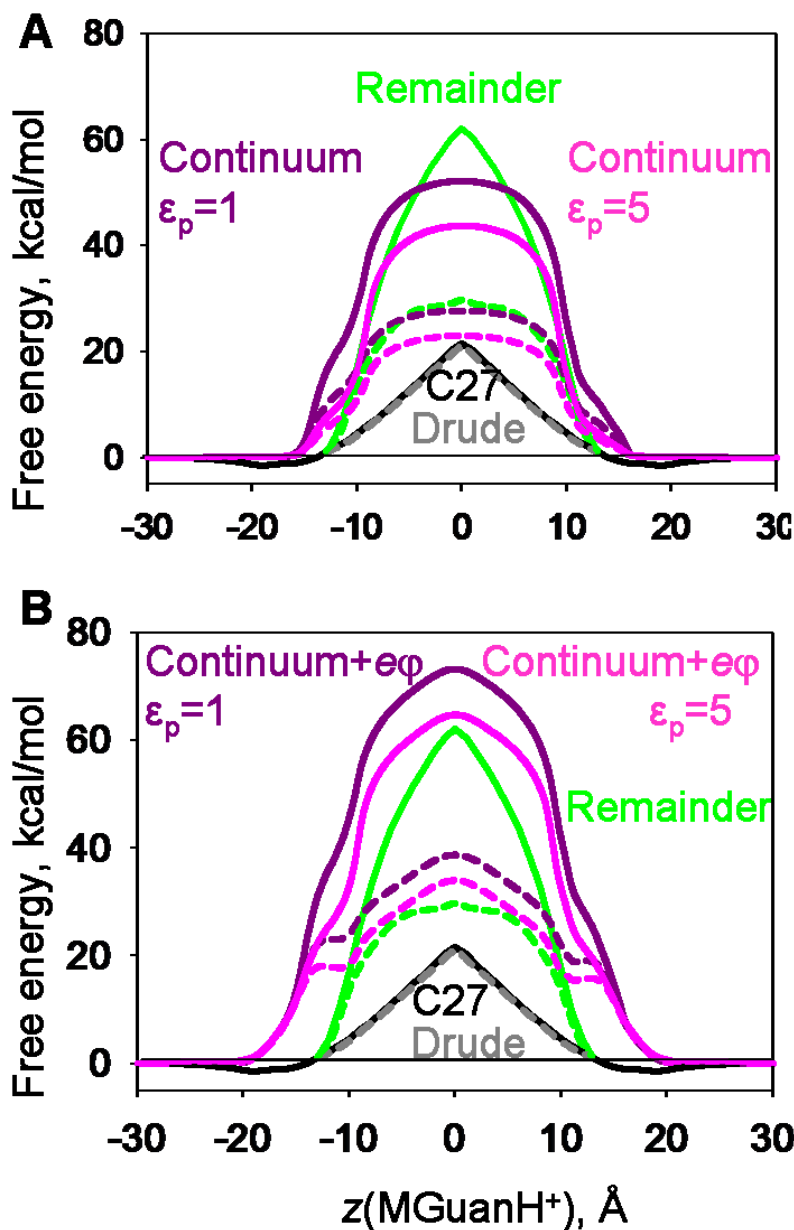
Figure S1. Comparison of total PMF (black and gray curves) and remainder terms (with polar components inside the membrane removed, see text) from non-polarizable C27 (solid curves) and Drude polarizable lipid tail C27+pol1 (dashed curves) all-atom MD simulations for a MGuanH$^+$ ion across a DPPC bilayer, with energy profiles from continuum membrane calculation models using membrane dielectric constant ε_m=1 (solid curves) or ε_m=2 (dashed curves) and 2 values of MGuanH$^+$ dielectric constant, ε_p. In panel (B) continuum membrane estimates were corrected for dipole potential contributions for C27 (for ε_m=1) or C27+pol1 (for ε_m=2) models.
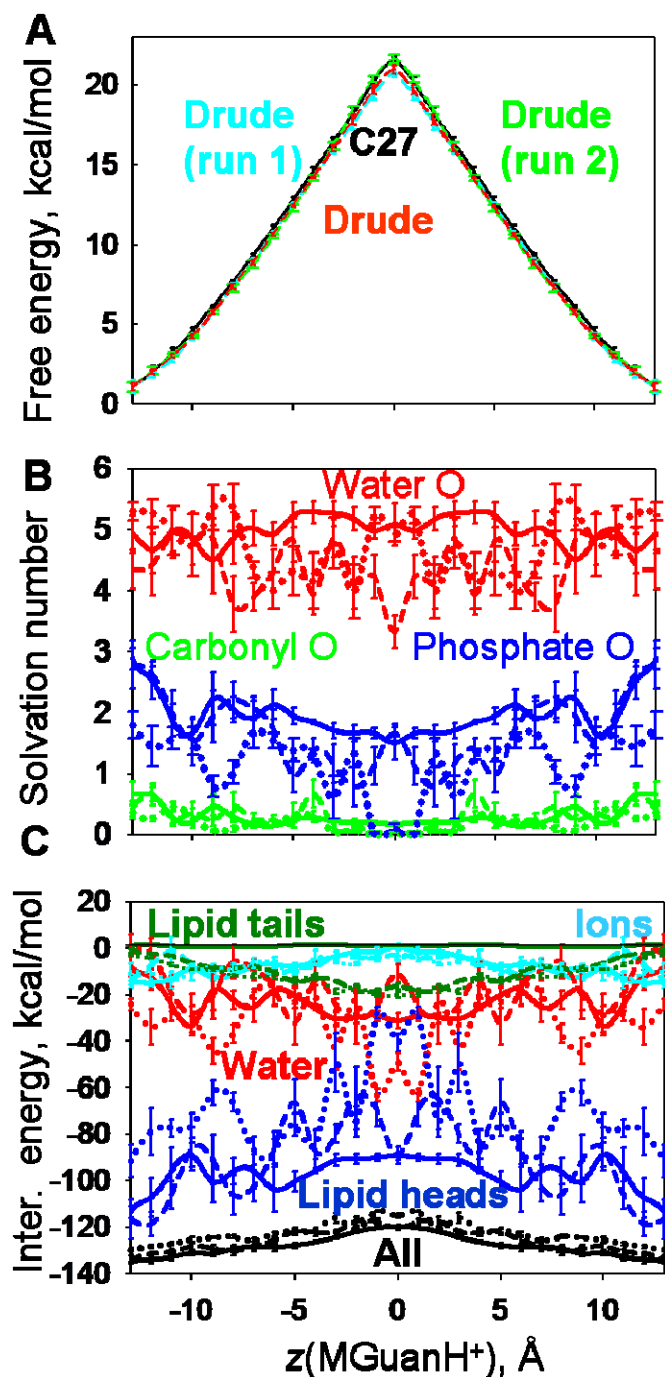
Figure S2. Free energy profiles (A), solvation numbers (B) and interaction energies (C) from all-atom MD simulations for MGuanH+ across a DPPC bilayer. In panels (B) and (C) solid lines are for C27, dashed and dotted are for C27+pol1 runs 1 and 2, respectively. In run 1 pre-equilibrated structures from non-polarizable simulations were used, whereas structures with no membrane deformation present were used as starting points for run 2. See ref. (21) for more information. All profiles have been symmetrized. Free energy profiles from C27+pol1 were referenced to those for C27 at |z(MGuanH+)|=13 Å. Solvation numbers represent the number of water, phosphate or carbonyl O atoms within 4.85, 4.55 or 5.00 Å of the guanidine C atom. Interaction energies in panel C have been calculated as energy differences and corrected for PME net charge artifacts (16). Error bars represent standard errors of the mean from block averaging.
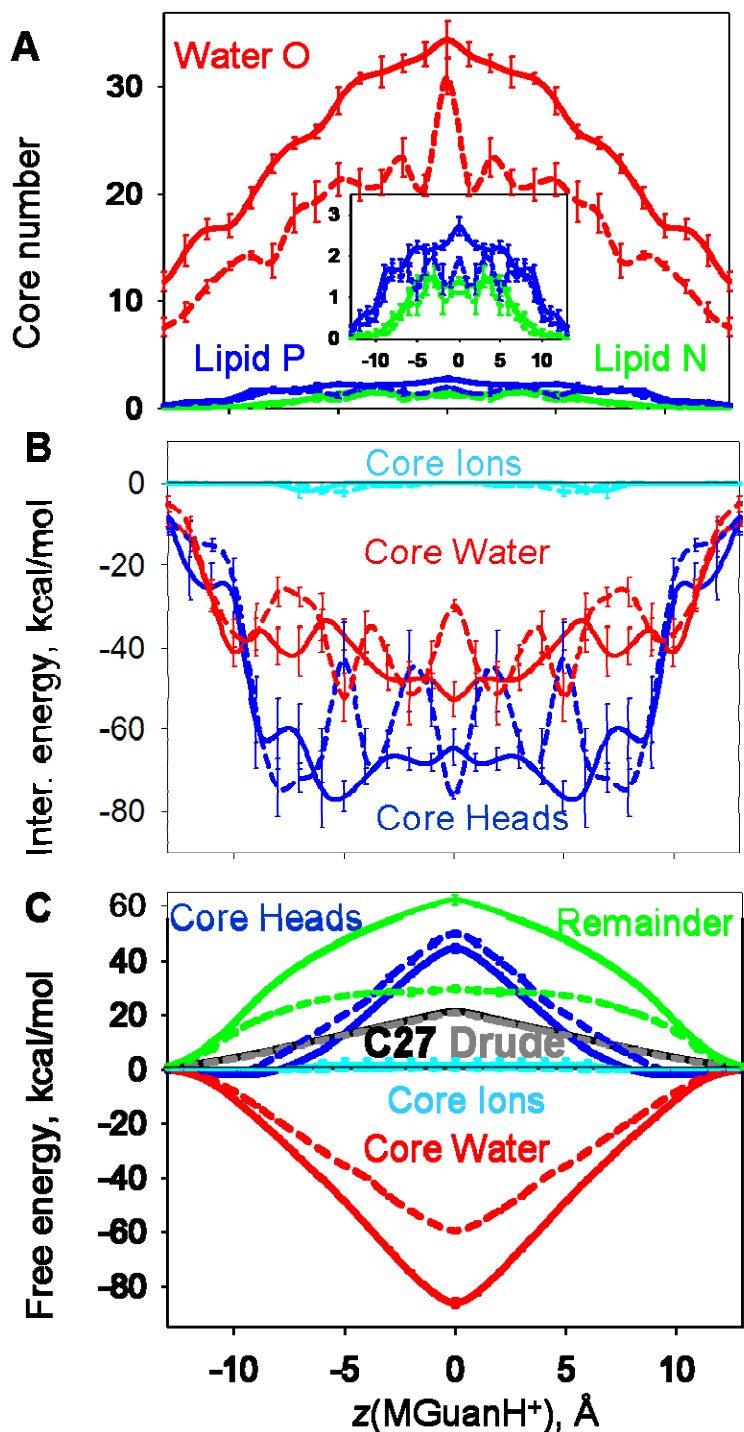
Figure S3. Number of polar species in membrane core defined as $|z| \leq 13$Å (A), interaction energies of MGuanH$^+$ with core membrane components (B) and free energy contributions to the total PMF (black and gray lines) from those core membrane components for MGuanH$^+$ across a DPPC bilayer. Solid lines are for C27 and dashed are for C27+pol1 (Drude) run 1 simulations. Error bars represent standard errors of the mean from block averaging.
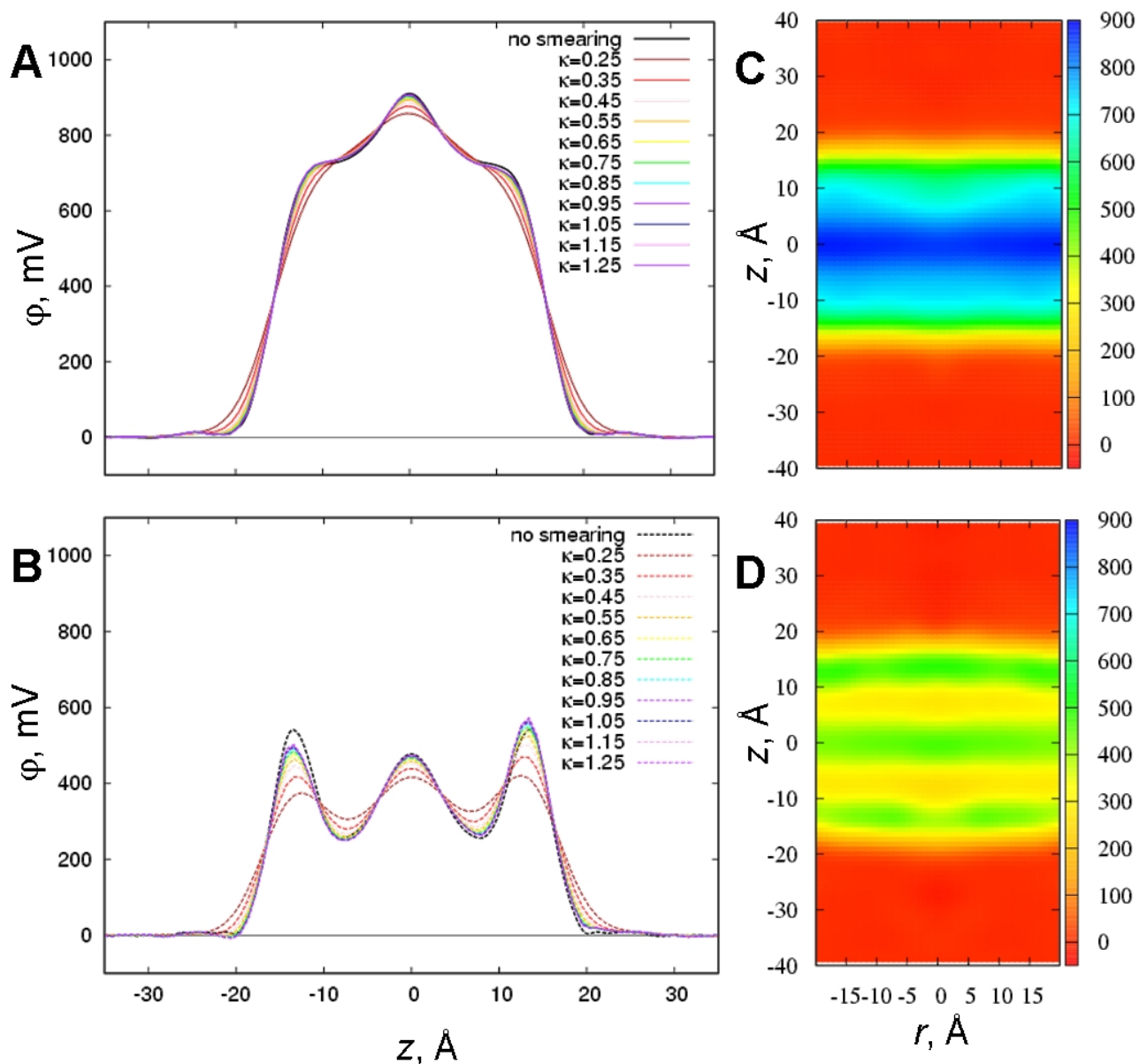
Figure S4. Electrostatic potential profiles for unperturbed DPPC bilayers using the PMEPOT module (28) of VMD (29). The effect of charge density smearing parameter κ on 1D potential profiles is shown for C27 (A) and C27+pol1 (B) models. The dipole potentials with no smearing (black curves) were obtained through the double integration of charged density (30). 2D potential profiles, as a function of z and the radial distance r from the z axis, are shown for C27 (C) and C27+pol1 (D) models using $\kappa=0.34$ Å^{-1}. The RMS errors for potential profiles corresponding to $\kappa=0.34$ Å^{-1} determined from block analysis are 4.5 mV for C27 and 7.3 mV for C27+pol2 models.
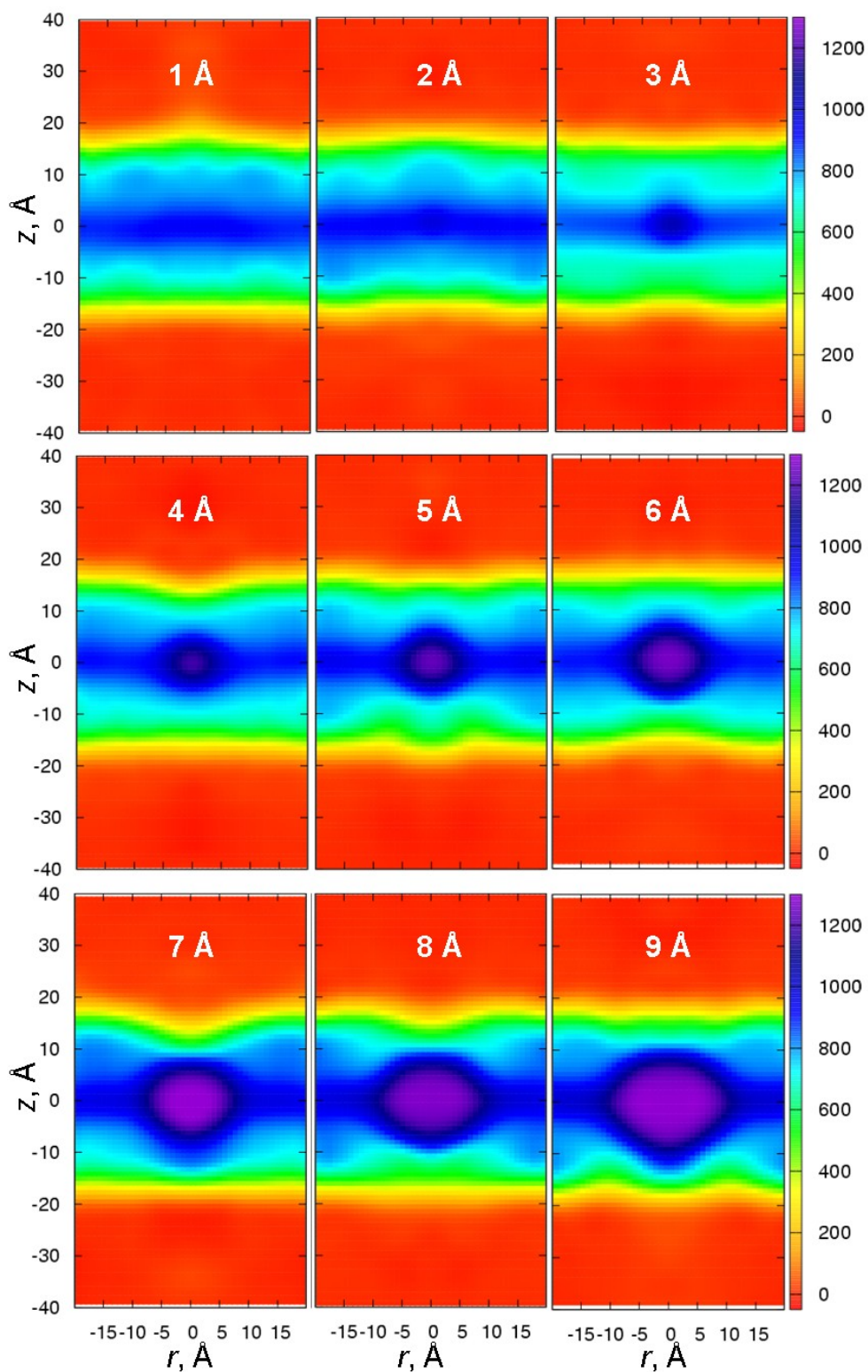
Figure S5. Electrostatic potential maps for DPPC bilayers with spherical voids of different radius, R_{sph}, (shown as white labels) from C27 simulations. These maps show the variation of the potential, φ (in mV, see color bars on the right), with z and the distance r from z axis. All potential maps are referenced to bulk aqueous solution and obtained using PMEPOT with smearing parameter 0.34 $Å^{-1}$.
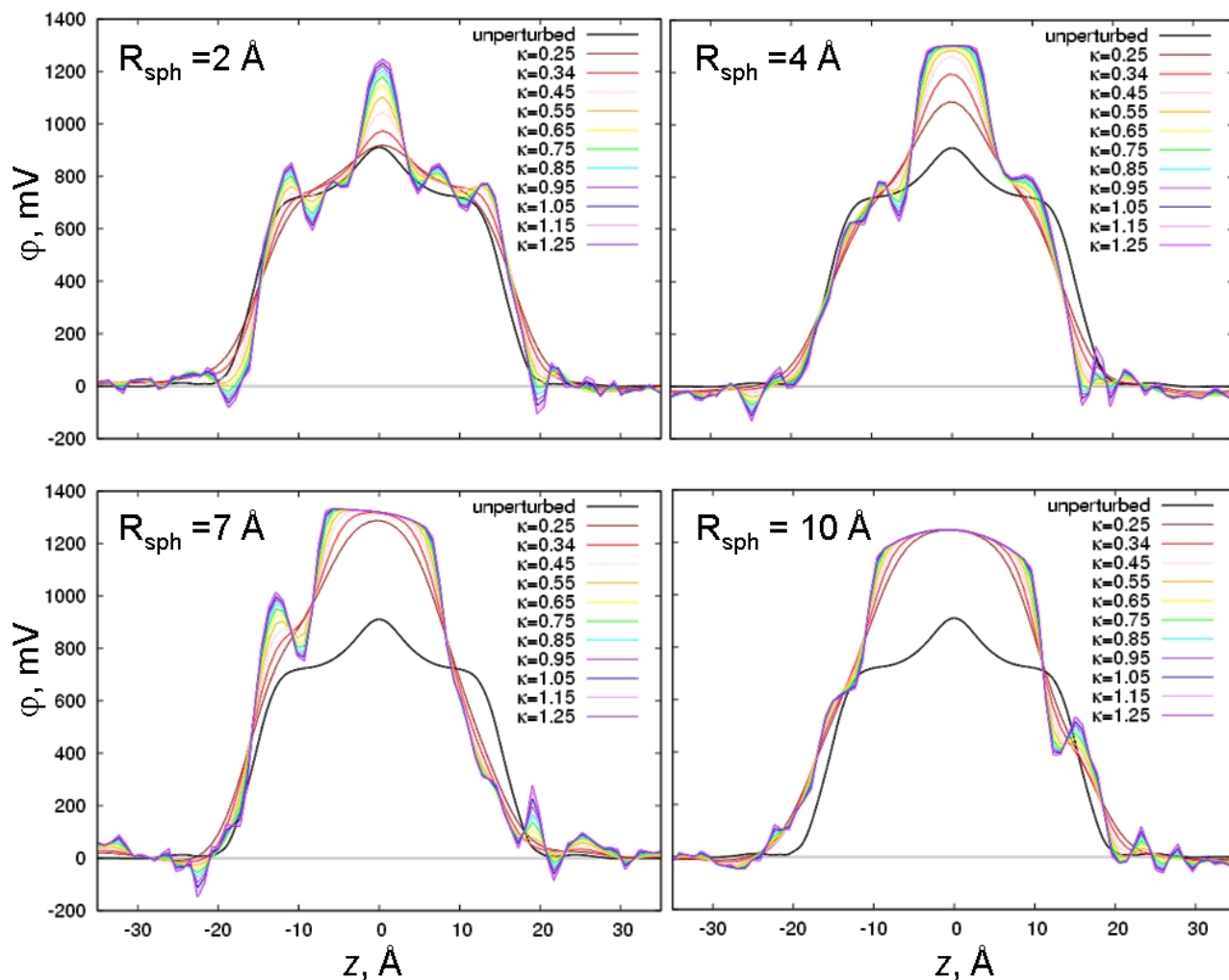
Figure S6. Electrostatic potentials for DPPC bilayers with spherical voids of different radius, R_{sph}, from C27 simulations. The 1D profiles show the variation in potential along the z axis as a function of charge density smearing parameter κ. All maps are referenced to bulk aqueous solution and obtained using PMEPOT. The RMS errors for potential profiles corresponding to $\kappa=0.34$ Å^{-1} determined from block analysis are $27 - 42$ mV. The dipole potential profiles for the unperturbed DPPC from charge density integration are shown as black lines.
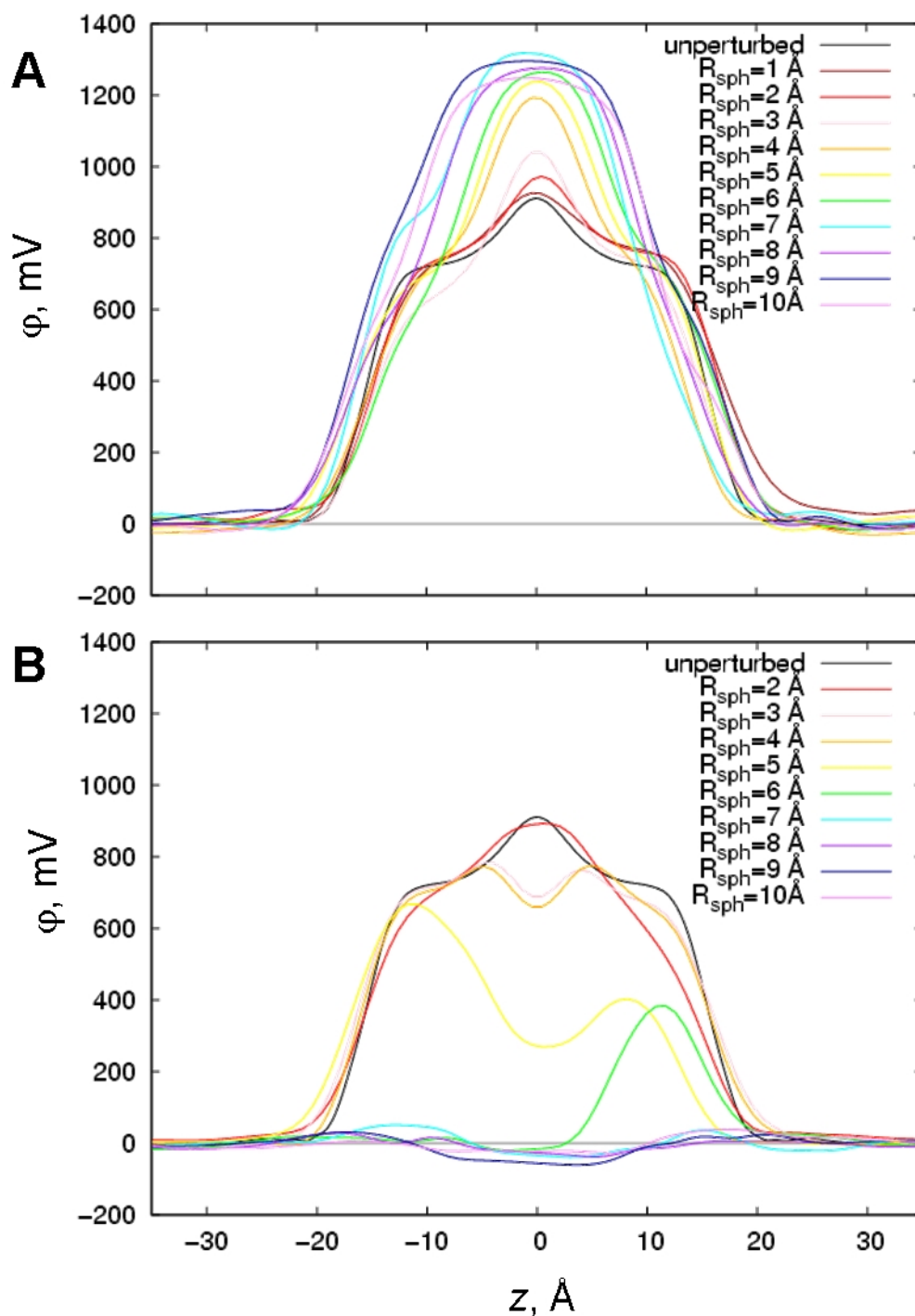
Figure S7. Potential profiles along the *z* axis for DPPC bilayers with hydrophobic (spherical voids, panel A) or hydrophilic defects (water-filled spherical cavities, panel B). All potential profiles are referenced to bulk aqueous solution and obtained using PMEPOT with $\kappa = 0.34$ Å^{-1}. The RMS errors for these potential profiles determined from block analysis are $18 - 54$ mV for hydrophobic and $8 - 42$ mV for hydrophilic defects. Potential profiles for unperturbed bilayers are shown as black lines. Note that profiles for smaller defects depend on the smearing parameter κ.
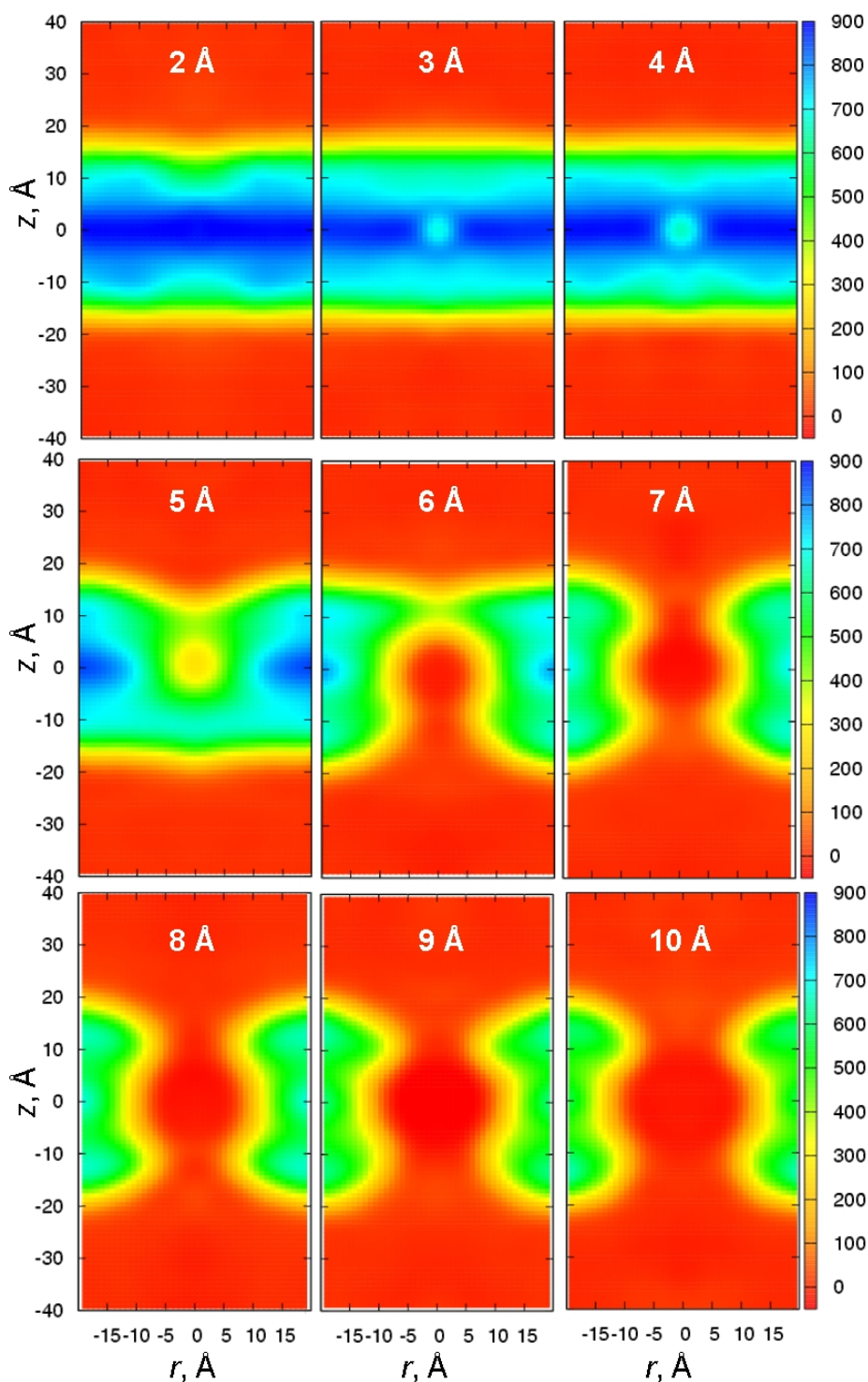
Figure S8. Electrostatic potentials for DPPC bilayers with water-filled spherical cavities of different radius, R_{sph} (shown as white labels), from C27 simulations. The 2D maps show the variation of the potential, φ (in mV, see color bars on the right), with z and the distance r from z axis. All maps are referenced to bulk aqueous solution and obtained using PMEPOT with 0.34 Å^{-1}. Note that for defects of radii 3–4 Å, where no substantial bilayer perturbation was observed, the effect on the potential is modest and localized to the membrane center where a drop from ~900 to ~600 mV occurs (see also Fig. S7B). This is partly associated with the formation of a water–hydrocarbon interface (~100 mV), but also due to the absence of a ~200 mV rise that would be seen without the defect (due to decreased hydrocarbon density at the bilayer center, see e.g. Fig. S4A).
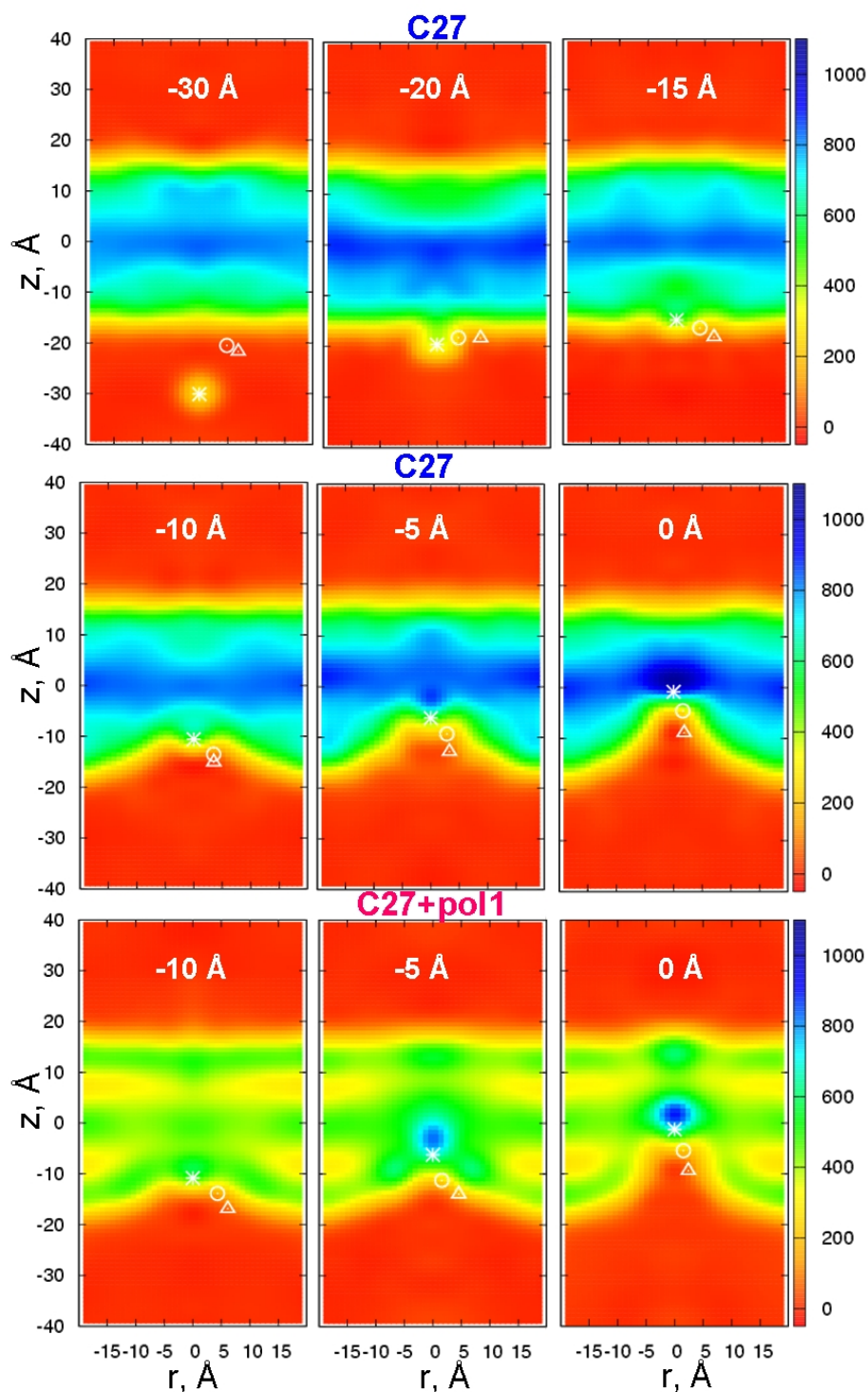
Figure S9. 2D electrostatic potential maps along z axis and distance *r* from z axis for different positions of MGuanH+, <*z*(ion)> (shown as white labels), across a DPPC bilayer from C27 and C27+pol1 simulations. Profiles were calculated using PMEPOT with κ=0.34 Å^{-1}. Electrostatic potential values (in mV, see color bars on the right) are referenced to bulk aqueous solution. The average positions of MGuanH+ guanidine C atom and its closest DPPC P and N atoms are shown as white asterisk, circle and triangle, respectively. Note that MGuanH+ contribution to the potential is present in these maps.
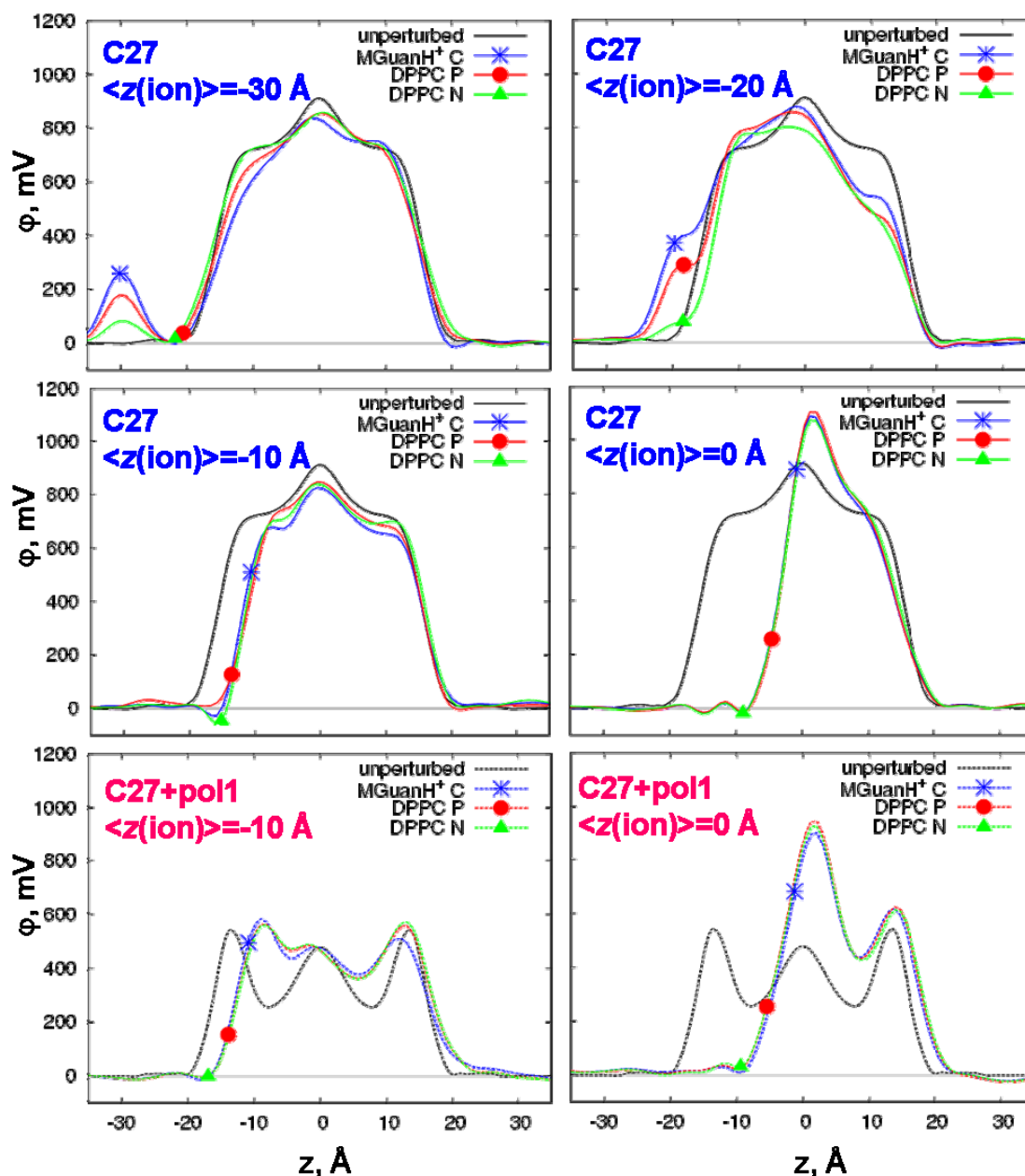
Figure S10. 1D electrostatic potential profiles along the z axis for MGuanH$^+$ transfer for several positions, $<z(ion)>$, across a DPPC bilayer from C27 (top and central panels) and C27+pol1 (bottom panels) simulations. Profiles were calculated for (x,y) passing through the average position (indicated on the curves) of the MGuanH$^+$ guanidine C atom (blue curve, asterisk), its closest phosphate P atom (red curve, circle) and N atom (green curve, triangle). Profiles were calculated using PMEPOT with $\kappa=0.34$ Å^{-1} and referenced to bulk aqueous solution. The RMS errors determined from block analysis are $22-45$ mV. Note that MGuanH$^+$ contribution to the potential is present in those profiles. Potential profiles for unperturbed bilayers are shown as black lines.
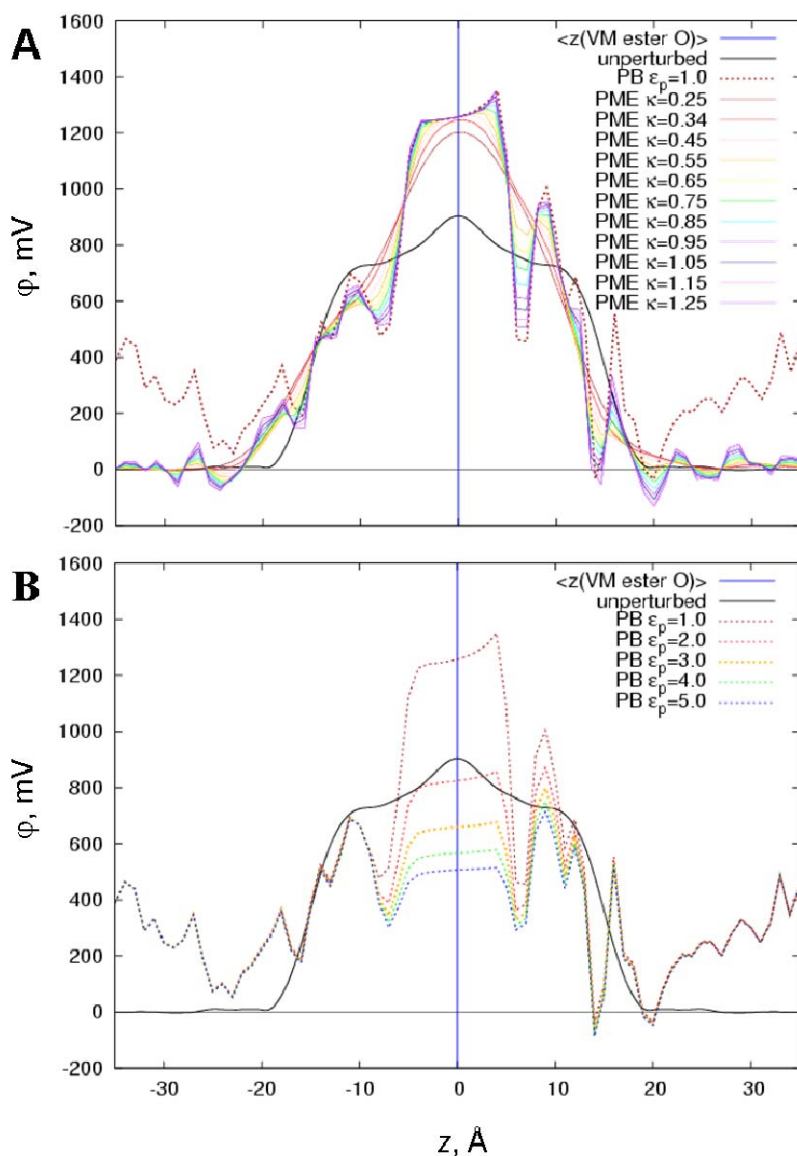
Figure S11. 1D potential profiles along the z axis for valinomycin (VM) constrained near the center of a DPPC bilayer from C27 simulations. Profiles were calculated using PMEPOT with zeroed VM charge contribution, using several values of κ and referenced to bulk aqueous solution (solid curves on panel A). The RMS error from block analysis for potential profile corresponding to $\kappa=0.34$ Å^{-1} is 51 mV. Potential profiles were also obtained with the same charge distribution using the PBEQ module of CHARMM and assigning different values of dielectric constant for protein atoms, ε_p (dotted curves on panels A and B). The dipole potential profiles for the unperturbed DPPC bilayer are shown as black curves. PBEQ profile for $\varepsilon_p = 1$ was referenced to PMEPOT profiles (A) at the average position of VM center (vertical blue line, defined as center of geometry of six ester carbonyl oxygen atoms). Profiles for $\varepsilon_p>1$ are matched to that for $\varepsilon_p = 1$ in bulk water (B).
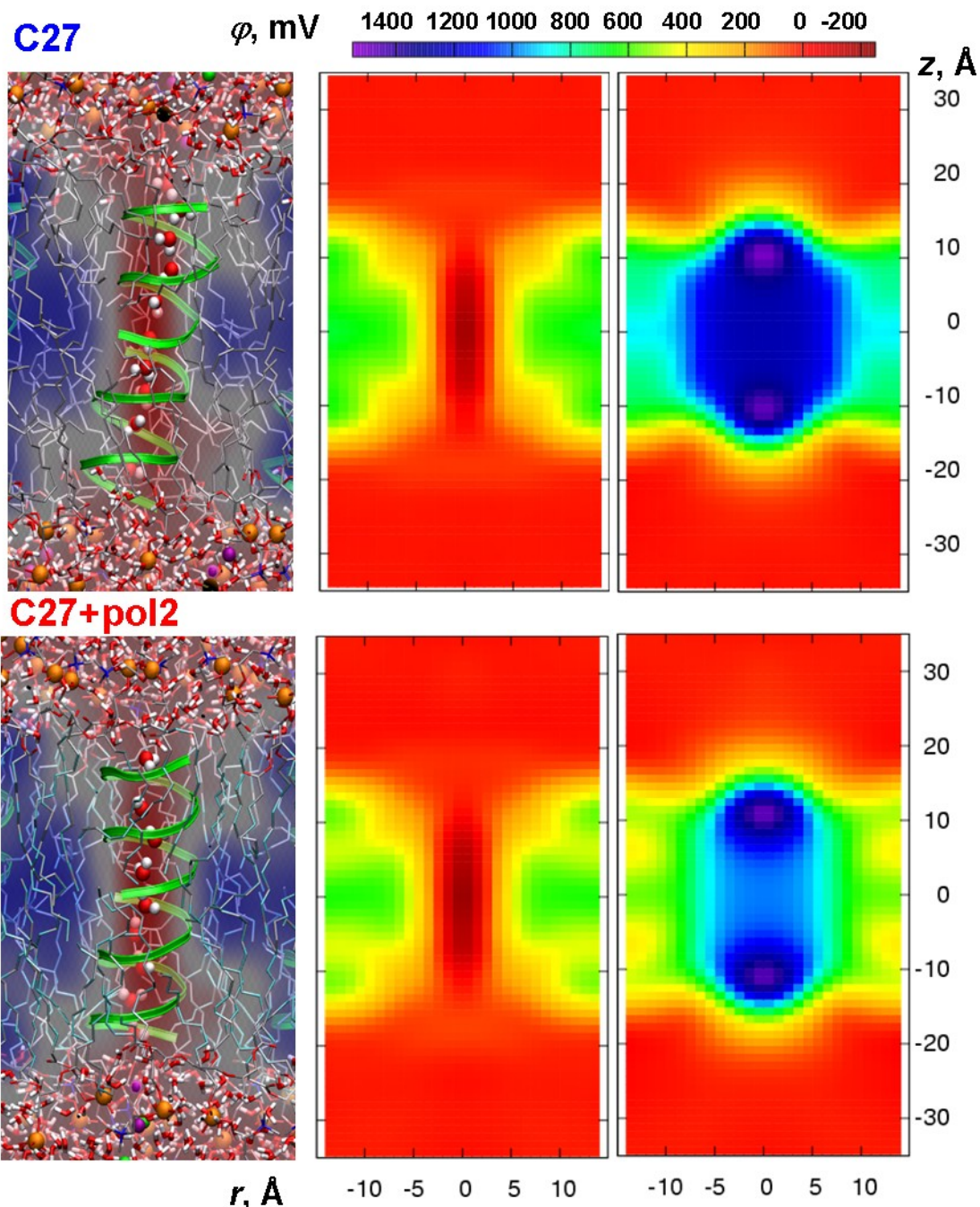
Figure S12. Snapshots (with superimposed averaged potential slices) and axially averaged 2D electrostatic potential maps for gramicidin A (gA) in a DMPC bilayer using non-polarizable C27 (top panels) and Drude polarizable C27+pol2 models (bottom panels). Potential maps in left and middle panels were calculated using all atom contributions and those in the right panels with the channel (gA and channel water) contribution excluded using PMEPOT with smearing factor κ=0.34 Å^{-1} and referenced to bulk aqueous solution. Note that new C27 tryptophan parameters (31) have been used for C27 gA simulations presented here.
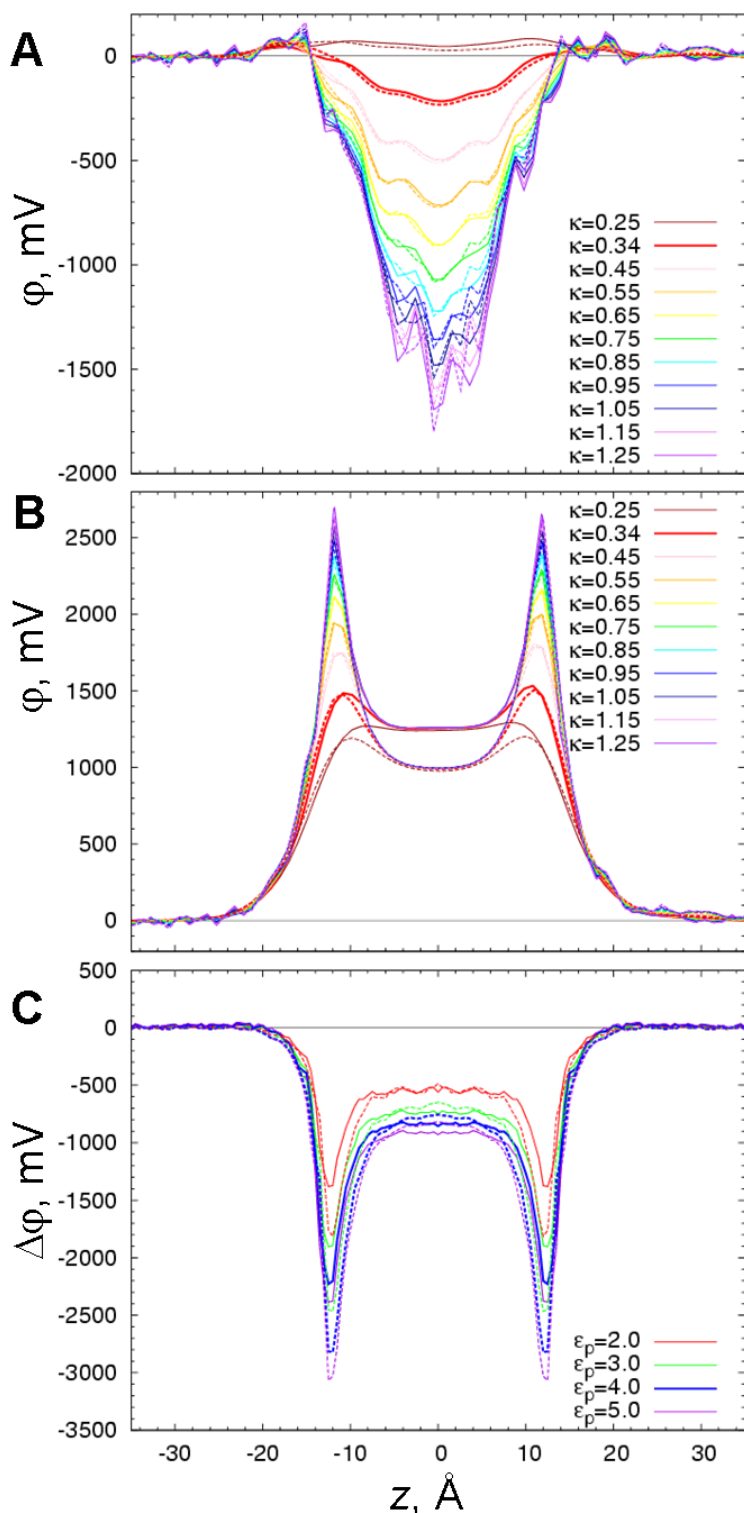
Figure S13. 1D potential profiles along the z axis for gramicidin A (gA) in a DMPC bilayer using non-polarizable C27 (solid curves) and Drude polarizable C27+pol2 models (dashed curves). Profiles in panels A and B were calculated with all atom contributions (A) or with the channel (gA and channel water) contribution excluded (B), using PMEPOT and several values of κ, referenced to bulk aqueous solution. The RMS errors for potential profiles corresponding to $\kappa=0.34$ Å^{-1} determined from block analysis are 11-16 mV for C27 and 16-50 mV for C27+pol2 models. Relative potentials, $\Delta\phi$, are plotted along the channel axis (aligned with the z axis) in panel C for different values of the channel dielectric constant, ε_p, relative to that for $\varepsilon_p=1$ (calculated using PBEQ).
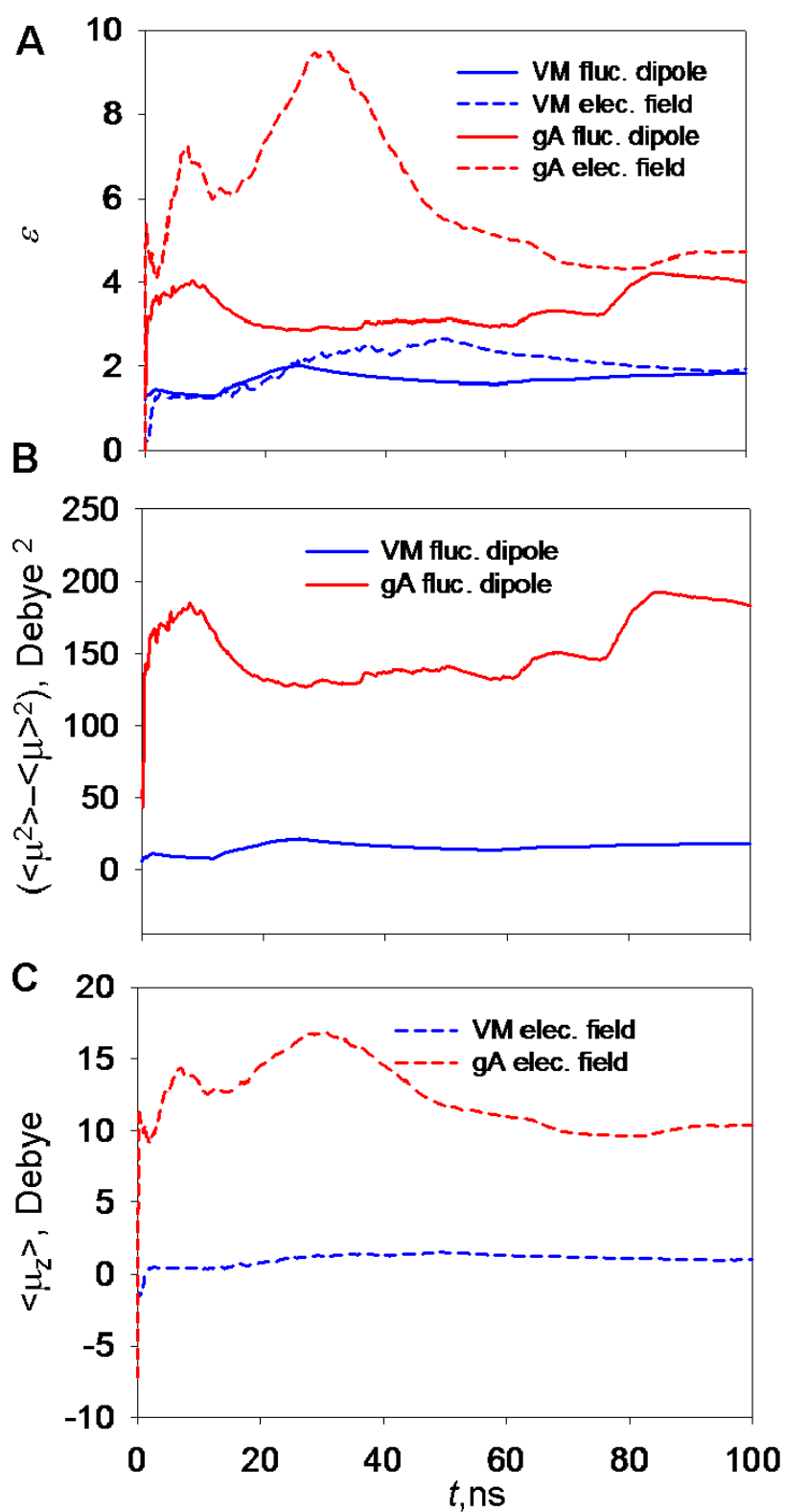
Figure S14. Time series of valinomycin (VM) and gramicidin A (gA) dielectric constant ε (panel A) estimated from calculations in vacuum as described in the Supporting Material text. Time series of dipole moment fluctuations, $(\langle\mu^2\rangle-\langle\mu\rangle^2)$, and the dipole moment component along the electric field direction, $\langle\mu_z\rangle$, which were used for ε estimation, are shown in panels B and C.